Characterization of Starburst Dendrimers by EPR. 4. Mn(II) as a Probe of Interphase Properties

M. Francesca Ottaviani,*,† Fabio Montalti,† Maurizio Romanelli,† Nicholas J. Turro,‡ and Donald A. Tomalia§

Department of Chemistry, University of Florence, 50121 Florence, Italy, Department of Chemistry, Columbia University, New York, New York 10027, and Michigan Molecular Institute, Midland, Michigan 48640

Received: November 2, 1995; In Final Form: April 16, 1996[⊗]

Mn(II) has been used as a probe to investigate the interacting abilities of the various ligand sites at the surface of starburst dendrimers (SBDs) at different protonation conditions, and as a function of generation (*G*), both for half- and full-generation SBDs (*n*.5-SBDs and *n*-SBDs, respectively). The computer-aided analysis of the electron paramagnetic resonance (EPR) spectra of Mn(II) provided information on the location of Mn(II) in the hydration layers of the internal and external SBD surface and on the physical status of water inside the dendrimer structure and at the surface/solution interface. Mn(II) did not show any interaction with the full-generation dendrimers and only interacted, at the second−third solvation shells, with the surface carboxylate groups (SBD-COO^-) of *n*.5-SBDs. Two main components were identified in the EPR spectra: (1) a minor component due to Mn(II) that is localized in the solvation layers of the internal and external SBD surface and is in fast exchange with the bulk solution. This Mn(II) fraction underwent a freezing transition at about 255 K; (2) a major component arising from complexation of Mn(II) with SBD-COO^- groups at the second solvation shell of the ions. The portion of solution that contained the Mn(II) complexes underwent a glass transition with a decrease in temperature. The complexation of Mn(II) was favored for later generation dendrimers ($G > 4.5$), at high pH and low Mn(II) concentrations.

Introduction

The supermolecular structures, termed dendrimers, have been attracting an increasing interest for the last decade, both as models of supramolecular biological and colloidal structures and as new materials for technical and industrial applications.[1−4] In the last few years, we focused attention on the poly(amidoamine) starburst dendrimers (SBDs), which are obtained by grafting amidoamine units to a central amino core.[5] Each shell of amidoamine units constitutes a generation (*G*). The amino-terminated SBDs are usually termed full generations, whereas the half-generations correspond to the termination with carboxylate (sodium gegenions) groups. The SBDs will be henceforth termed, for simplicity, *n*-SBDs and *n*.5-SBDs for the full and half generations, respectively. The nomenclature used in this paper for the SBDs is the one generally accepted for the dendrimers.[1−4] Chart 1 shows, as an example, a bidimensional projection of the 3- and 3.5-SBDs used in this work.

Interest in these SBDs mainly resides in the resemblance of their internal structure to biomacromolecules, such as globular proteins and enzymes, and of the external layers and interfacial properties to ordered systems, such as micelles, vesicles, and membranes.

Molecular simulation of the structure of the SBDs[6] revealed a dramatic change in morphology at $G = 4$ (and by inference for $G = 4.5$): the so-called earlier generations ($G < 4$ or 4.5) possess an open structure and an ellipsoidal shape, whereas the later generations ($G > 4$ or 4.5) are characterized by a closed structure with a densely packed surface and a spherical shape.

Characterization of the properties of the SBDs has been carried out mainly by means of analytical methods and photophysical and spectroscopic studies.[5,7−14] Recently, electron paramagnetic resonance (EPR) of nitroxide radicals has been used to investigate the interacting abilities of surface external and internal ligand groups of *n*.5-SBDs[12] and the aggregation process of a positively charged nitroxide surfactant in the presence of the *n*.5-SBDs.[13] However, the nitroxide group is apparently too large to enter inside the dendrimer structure, and therefore, EPR only monitors directly the occurrence of interactions between the polar nitroxide groups and polar or charged groups at the SBD external surface. Conversely, paramagnetic metal ions may enter the dendrimer structure and bind to both internal and external ligand groups. We have already investigated the complexes that are formed by adding Cu(II) to solutions of *n*.5-SBDs with different sizes and under various experimental conditions (pH, temperature, concentration).[14] The

CHART 1

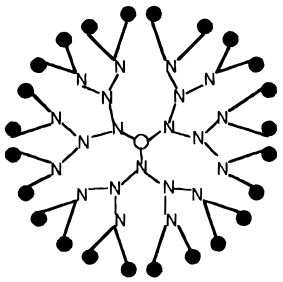

3- or 3.5-SBD

N-N ⇒ N-CH_2-CH_2-CO-NH-CH_2-CH_2-N

●-N ⇒ H-N = full generation

(Na^+) $^-$OOC-CH_2-CH_2-N = half generation

† University of Florence.
‡ Columbia University.
§ Michigan Molecular Institute.
[⊗] Abstract published in *Advance ACS Abstracts,* June 1, 1996.

S0022-3654(95)03261-8 CCC: $12.00

similarity between the poly(amidoamine) dendrimers and biomacromolecular structures (proteins, and enzymes) has been verified on the basis of the correspondence between the EPR spectra recorded for the Cu(II)−dendrimer systems and the EPR spectra reported in the literature for Cu(II)−protein or enzyme complexes.

The present study is a natural extension of this previous work, since it reports on the use of the Mn(II) ion, which provides information complementary to those obtained by means of the Cu(II) ion. In particular, the solution EPR spectra of Mn(II) exhibit a marked dependence on the environmental conditions, whereas the spectra of Cu(II) ions provide information on the complexes directly formed with surface ligand groups. EPR spectra of Mn(II) are extremely sensitive to symmetry changes around the paramagnetic center. Indeed, most of the EPR studies on fluid solutions containing Mn(II) have been carried out to investigate ionic interactions in inorganic systems and in Mn-containing soluble materials.[15−20] It is well-known that the interacting ability of Mn(II) toward amino, amide, or carboxylate groups is more selective than the complexing ability of Cu(II) toward the same ligands. Consequently, Mn(II) is more informative than Cu(II) about the different interacting abilities of the various ligand groups, and it works better as a probe of environmental properties when compared to Cu(II). Thus, the aims of the present study are as follows: (1) the analysis of the location of Mn(II) outside and/or inside the dendrimer structure and the different interacting abilities of the various ligand sites at the dendrimer surface; (2) the physical status of water inside the dendrimer structure and at the surface/solution interface.

Mn(II) can be helpful in addressing these issues, since the computer-aided analysis of the EPR spectra provides structural and dynamic information, in addition to information concerning the partitioning of the probe in different environments. For instance, the literature provides many examples of the use of Mn(II) to study water finely dispersed in restricted spaces by means of EPR spectral analysis.[21−25]

This study is carried out as a function of various experimental parameters, such as dendrimer generation, pH of the solution, temperature, and concentration of both the probe and the dendrimers.

Analysis of the EPR Spectra

The spectroscopic ground state of Mn(II) is ^{6}S, with total spin $S = {}^5/_2$, and nuclear spin $I = {}^5/_2$ that gives rise to the usual sextet of lines in the EPR solution spectra at room temperature. The appropriate spin Hamiltonian for such system is

$$\hat{H} = g\beta\bar{B}\hat{S} + a\hat{I}\hat{S} + D[S_z^2 - ({}^1/_3)S(S+1)] + 2E(S_x^2 - S_y^2) \quad (1)$$

In the first term, the Zeeman Hamiltonian for the interaction between the electron spin and the magnetic field (B, magnetic field; β, Bohr magneton), the g factor is isotropic and close to the free electron value ($g = 2.0023$); the hyperfine (hpf) coupling constant a, in the second term for the coupling between the electron and the nuclear spins, is also isotropic and changes slightly with the electronegativity of the coordinated ligands. Both parameters may be exactly evaluated in the computation of the spectral line shape (see below), but they give almost no structural information. The last two terms in the spin Hamiltonian represent the so-called zero-field splitting (ZFS) interaction, which may be more correctly written as **S.D.S**. The ZFS arises from electron spin−electron spin coupling for $S > {}^1/_2$ systems. **D** is a traceless tensor described by an axial parameter D and an orthorhombic parameter E (for axial symmetry, $E = 0$). Since the ZFS accounts for the separation of the spin levels due to an unsymmetrical ligand field on the ion, it represents the major structure-sensitive term. In solution, if rotation is sufficiently fast, the line positions are not affected by the ZFS. On the contrary, the time modulation of the ZFS parameters is the main electron spin relaxation mechanism. Both molecular reorientations and distortions caused by collisions with solvent or ligand molecules may cause spin relaxation.[26−28] The main contribution to the line width of the EPR spectra at room temperature, from relaxation theory, is:[29−31]

$$T_2^{-1} = -\left(\frac{\mathbf{D:D}}{5}\right)\left[16\frac{\tau_c}{1+\omega_0^2\tau_c^2} + 56\frac{\tau_c}{1+4\omega_0^2\tau_c^2}\right]$$

where **D:D** is the inner product of the ZFS tensor, ω_o is the electron spin resonance frequency and τ_c is the correlation time for motion, which may be either the rotational diffusion or any other motional fluctuation that affects the ZFS tensor.[29] If a Brownian rotational diffusion is assumed, the correlation time for motion depends on the viscosity/temperature ratio:

$$\tau_c \propto \eta/T \quad (3)$$

The relaxation theory indicated the dependence of the line width on the **D:D** parameter. Distortions from the cubic symmetry of the Mn−aquo complex due to replacement of the water molecules in the first solvation shell with ligand groups induces a marked increase of the **D:D** parameter, which, in turn, causes a line broadening so large as to lead to a unobservable EPR signal.[19] Therefore, the fraction of Mn(II) involved in complexation in the first solvation layer may escape detection. Conversely, changes in the outer solvation sphere simply broaden the line width of the hpf components, and the evaluation of the broadening has been used to extract structural and dynamic information on the system under study.[27−28] However, line broadening may also arise from the increase in microviscosity around the paramagnetic ion.

The line width, based on the eq 2 and on the dependence of τ_c on temperature (eq 3), increases with the decrease in temperature at $\omega_o^2\tau_c^2 \ll 1$ ($T_2^{-1} \propto \tau_c \propto \eta/T$) up to reach a maximum at $\omega_o^2\tau_c^2 = 1$ and then decreases with further decreases in temperature at $\omega_o^2\tau_c^2 \gg 1$ ($T_2^{-1} \propto 1/\tau_c \propto T/\eta$).[30,31] Upon freezing of Mn^{2+} solutions, the solute was separated from the crystallized solvent. The spectrum of the solid Mn^{2+} salt is too large to be detected (broad distribution of **D:D** parameters). But, water solutions in microetherogeneous systems do not freeze and a glass transition is found, which allows the evaluation of the correlation time for motion at the maximum as $\tau_c = \omega_o^{-1} = 1.7 \times 10^{-11}$ s. This value may be therefore taken as the basis for the calculation of the temperature dependence of the correlation time. The EPR spectra of Mn(II) in a glassy matrix are characterized by a doublet of lines between the main hpf lines, due to the so-called forbidden transitions ($\Delta m_I \neq 0$).[32]

In the system studied in this work, only a fraction of Mn(II) showed a glass transition, due to the interaction with the SBD surface. The freezing transition occurred in the temperature region of the line width maximum and did not allow its detection. Consequently, only spectral simulation by means of suitable programs should provide the values of the correlation time for motion and of the other magnetic and structural parameters that characterize the EPR line shape of Mn(II) in SBDs solutions at room temperature.

We used the calculation program of Luckurst and Pedulli,[30,31] and modified by Romanelli and Burlamacchi.[33,34] The main steps in the calculation are as follows:

(a) The use of the static Hamiltonian (eq 1) provides the positions of the 30 transitions arising from $S = {}^5/_2$ and $I = {}^5/_2$. The hyperfine interaction was assumed as a second-order perturbation with respect to the electron Zeeman interaction.

(b) The evaluation of the elements of the relaxation matrix (Redfield matrix) is carried out through the spectral densities at the frequencies 0, ω_o, and $2\omega_o$ for each of the five electron transitions, coupled to the other transitions that contribute to alter the population of the spin levels.

(c) The relaxation matrix for each transition in a chosen magnetic field range is diagonalized. The eigenvalues correspond to the line widths, whereas the eigenvectors correspond to the related intensities.

The input parameters are (i) the $\langle g \rangle$ and $\langle a \rangle$ values. In the Mn−SBD system, $\langle a \rangle$ only underwent a small increase with the increase in environmental polarity, due to the insertion of Mn(II) in the SBD structure (see below); (ii) τ_c; and (iii) D. The analysis of the computed line shapes and their comparison with the experimental spectra allowed the evaluation of the parameters for each experimental measurement.

Experimental Section

All the aqueous solutions used in this work were prepared with doubly distilled water filtered through Millipore filters.

The poly(amidoamine) family of starburst dendrimers employed in this study has been synthesized as described in previous papers.[5] The half-generations were obtained by hydrolyzing the methyl ester-terminated generations with stoichiometric amounts of NaOH in methanol to obtain sodium carboxylate external groups with sodium gegenions. Both the *n*-SBDs and the *n*.5-SBDs were thoroughly purified from water solutions. Water solutions of the SBDs were prepared and stored under nitrogen at about 278 K. The present study reports on results from water solutions of 3-, 3.5-; 5-, 5.5-; and 7-, 7.5-SBDs. The number of surface groups, the molecular weights, and the initial concentrations in external NH_2 or COO^- groups (SBD-COO^-) are the following:

generation	surface groups (sg)	MW	init concn (sg M)
3	12	2414	0.34
3.5	24	4671	1.06
5	48	10633	0.43
5.5	96	19661	0.83
7	192	43508	0.43
7.5	384	79621	0.39

The solutions of the SBDs were diluted with water and Mn(II) solutions to obtain the concentrations reported in the Results and Discussion section for the various experimental measurements.

Water solutions of $Mn(ClO_4)_2 \cdot 6H_2O$ (Fluka, used as received) were prepared at a concentration of 10 mM and diluted as necessary. Freshly prepared Mn(II) solutions were used for each series of samples, since aged solutions showed partial hydrolysis of the Mn−aquo ions. The Mn(II) solutions were mixed with the SBD solutions in the appropriate ratios (see text and captions of the figures). The EPR spectra were recorded immediately after preparation of the samples, by inserting a 200 μL solution in a quartz tube (2 mm i.d.).

The variation of pH was accomplished by adding suitable amounts of HCl (Merck, used without any further purification) at an initial concentration of 1.2 M.

Measurements of the variation of signal intensity from pure Mn(II) solutions to solutions containing 7.5-SBD were achieved by using a flat cell fixed in the EPR cavity and a flow-and-stop procedure, which guarantees the recording of the spectra under the same experimental conditions.

The EPR spectra were recorded by means of a Bruker 200D spectrometer operating in the X band, interfaced with Stelar software to a PC-IBM computer for data acquisition and handling. The temperature was controlled with the aid of a Bruker ST 100/700 variable-temperature assembly. Magnetic parameters were measured by field calibration with the DPPH radical ($g = 2.0036$).

The EPR spectra computed by changing parameters in the extent of 10% provided unappreciable differences in the computed line shape. This value was therefore taken as the precision limit in the evaluation of the spectral parameters.

The pH was measured with a Sentron-2001 pH meter[35] equipped with a microelectrode to permit the measurement of small volumes (0.2 mL).

TABLE 1: pK_b Values (Accuracy 5%) for the Various Sets of Equivalent Basic Groups (eq.gps) of Some Representative SBDs[a]

G	set of eq.gps	no. of eq.gps	p$K_{b,min}$	p$K_{b,max}$	pH
3	NH_2 external layer	12	−11.5	−9.0	8.5
3	NR_3 at $G = 2$	6	−7.6	−6.1	5.5
3	NR_3 at $G = 1$ and core	4	−5.6	−5.3	3
5	NH_2 external layer	48	−13.2	−8.5	8
5	NR_3 at $G = 4$	24	−7.1	−5.7	5
5	NR_3 at $G = 3$, 2, 1, and core	22	−5.4	−3.4	2
5.5	NR_2, R′ at $G = 5$	48	−9.0	−6.9	7
5.5	NR_3 at $G = 4$	24	−6.6	−4.8	4.5
5.5	NR_3 at $G = 3$	12	−4.7	−4.0	3.5
5.5	NR_3 at $G = 2$, 1, and core	10	−3.9	−3.4	3
5.5	COO^- external layer	48	−3.9	−1.5	1.5

[a] The minimum and the maximum pK_b values (p$K_{b,min}$ and p$K_{b,max}$, respectively) for each set are listed. The pH values for protonation of each set are also reported.

Results and Discussion

Basicity of the Starburst Dendrimers. The study of the interactions between Mn(II) and the SBD surface groups requires knowledge of the basicity of these dendrimers.

The SBD macromolecules are polyprotic bases, which contain sets of equivalently basic groups. The variation of pH as a function of the HCl concentration was calculated by means of a program (PHSIMULA) that provides the pK_b values (accuracy 5%) for the various sets of equivalent groups, listed in Table 1 together with the pH values at which protonation of each set occurs.

The pK_b values listed in Table1 were consistent with the following conclusions: (i) Protonation of the various sets of equivalent groups occurs in the sequence: $NH_2 > NR_3 > COO^-$. (ii) The more external the basic groups, the easier the protonation occurs, with the exception of the carboxylate groups of the *n*.5-SBDs. (iii) Protonation is preferred for earlier generations with respect to later generations. (iv) Protonation is preferred for full generations with respect to half-generations. (v) The basic groups belonging to the most internal sets differ very slightly from each other in their basic abilities.

Most of the results discussed in the next sections refer to pH = 4 and pH = 7. The choice of these two pH values was determined by the different range of protonation involved at these pH values. In detail, at pH = 7 the protonation of the first layer of NR_3 groups occurs, whereas at pH = 4 more internal NR_3 layers are also protonated. This behavior facilitated identification of the location of Mn(II) in the SBD structure.

Variation of the Intensity of the EPR Signal for the Formation of Mn−SBD Complexes. The spectra of Mn^{2+} in

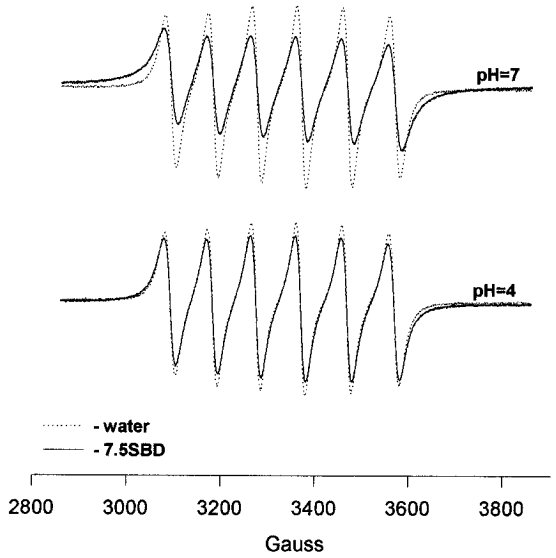

Figure 1. EPR spectra (298 K) of Mn^{2+} solutions (2×10^{-4} M) in the absence (dashed lines) and in the presence (full lines) of 7.5-SBD; [SBD-COO^-] = 0.37 M. The spectra were obtained with the flat cell fixed in the EPR cavity and a stop-and-flow procedure.

the absence and in the presence of full-generation dendrimers were completely equivalent to each other (results not shown), both in the relative intensities and in the line shapes. This was interpreted in terms of no interaction between Mn(II) ions and full-generation dendrimers, as inferred by EPR measurements. Therefore, results from Mn(II) solutions in the presence of full-generation dendrimers will not be discussed further. On the contrary, the EPR line shape of the system Mn(II)−7.5-SBD showed marked modifications in both the relative line widths and heights of the hpf lines, if compared to the spectrum in the absence of the dendrimer. This is shown in Figure 1 for Mn^{2+} (2×10^{-4} M) solutions in the absence (dashed lines) and in the presence (full lines) of 7.5-SBD (0.37 M), and at pH = 7 and 4 and $T = 298$ K. The spectra were obtained with the flat cell fixed in the cavity, as described in the Experimental Section.

Since the main difference between the half and the full generation is the external layer of COO^- groups and NH_2 groups, respectively, we concluded that Mn(II) had no interacting ability toward the amino groups of the SBDs, whereas it interacted significantly with the SBD-COO^- groups.

As pointed out in the section on the Analysis of the EPR Spectra, the direct complexation of Mn^{2+} (water substitution in the first solvation sphere) leads to such an increase in the **D:D** parameter (**D:D** > $(4-5) \times 10^5$ G^2) (=increase in line width) to lack detection of the EPR signal. The integrated intensities of the signals in Figure 1 were almost the same in the absence and in the presence of the dendrimers. This meant that the ZFS parameters were not as large as expected in case of direct complexation of Mn(II) with the COO^- groups: only water substitution in the second solvation shell of the ions accounts for the line broadening shown by the spectra in Figure 1.

The next sections deal with the analysis of the line shape variations of the systems Mn(II)−*n*.5-SBDs under various experimental conditions.

Computer-Aided Analysis of the EPR Spectra of Mn(II)−*n*.5-SBDs: Variation of Generation at pH = 4 and pH = 7. Figure 2 shows the experimental (full lines) and the computed (dashed lines) EPR spectra of Mn(II) solutions (2×10^{-4} M) in pure water and in 3.5-, 5.5-, and 7.5-SBDs (0.37 M in SBD-COO^-) recorded at 298 K. Figure 2a shows the spectra at pH = 4, whereas in Figure 2b the spectra at pH = 7 are reported.

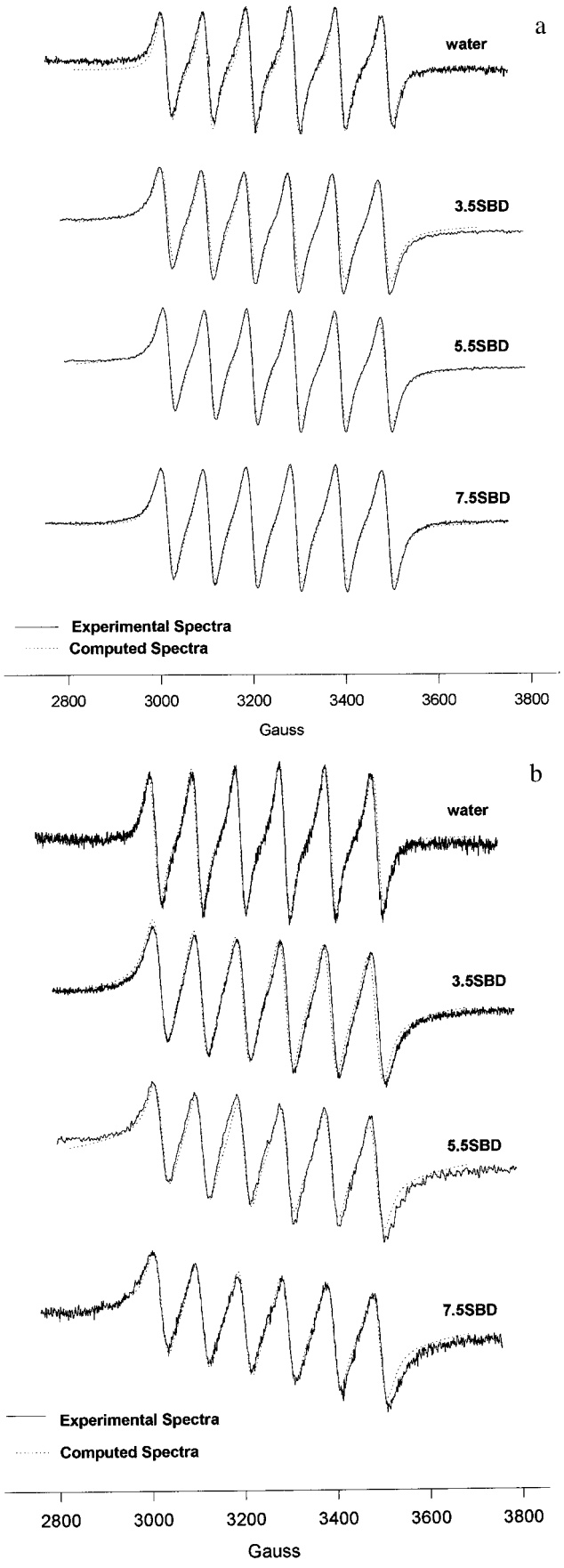

Figure 2. Experimental (full lines, 298 K) and computed (dashed lines) EPR spectra of Mn(II) solutions (2×10^{-4} M) in pure water and in 3.5-, 5.5-, and 7.5-SBDs (0.37 M in SBD-COO^-). (a) pH = 4; (b) pH = 7.

TABLE 2: Parameters Used for the Computation of the EPR Spectra[a]

generation	pH	signal	τ_c (ps)	**D:D** (G^2)	$\langle a \rangle$ (G)	rel %
0	7	A	7	24 000	96.4	100
2.5	7	A	10	30 000	92.8	20
		B	(7)	250 000	(92.8)	80
5.5	7	A	10	30 000	92.5	15
		B	(7)	250 000	(92.5)	85
7.5	7	A	10	30 000	94.2	15
		B	(7)	250 000	(94.2)	85
0	4	A	7	24 000	95.0	100
3.5	4	A	8	30 000	93.6	30
		B	(7)	250 000	(93.6)	70
5.5	4	A	8	30 000	93.3	33
		B	(7)	250 000	(93.3)	67
7.5	4	A	8	30 000	95.0	40
		B	(7)	250 000	(95.0)	60

[a] Correlation time for motion, τ_c (±5%), ZFS parameter, **D:D** (±10%); isotropic hyperfine coupling constant, $\langle a \rangle$ (±5%); and relative percentages of the components A and B (±5%).

Consistent with the data described in the previous section, the spectra at pH = 7 showed larger modifications if compared to the spectrum in the absence of the dendrimers.

The attempts to compute the experimental spectra by considering a single spectral component constituting the EPR signal were unsuccessful. The use of two contributions, termed spectrum A and spectrum B, allowed us to obtain a rather good fitting (as shown in Figure 2) between the experimental and the computed signals and to evaluate the spectral parameters with satisfying accuracy. An apparent misfit occurs for low-intensity signals, mainly because of the baseline slope. The fitting could be partially improved by adding several contributions, but this determined a lack of precision in the evaluation of the spectral parameters and in the interpretation of the system behavior. We therefore assumed that the Mn^{2+} ions were located in two different environments in slow exchange rate in the EPR time scale (10^8-10^9 s^{-1}). Thus, the experimental spectra were computed by calculating the two components, A and B, and by adding them at certain relative percentages to reproduce the experimental line shapes. Table 2 reports the parameters used for the computation of the spectra in Figure 2, that is, the correlation time for motion, τ_c, the ZFS parameter, **D:D**, the hpf coupling constant, $\langle a \rangle$, and the relative percentages of the two components A and B. For spectrum B, the τ_c and the $\langle a \rangle$ parameters were slightly significant and are reported in parentheses, since the precision in their determination largely decreased because of the broadening due to the large ZFS parameter. The data in Table 2 are consistent with the following interpretation:

(1) Spectrum A of the SBD solutions shows parameters close to the parameters calculated for Mn(II) solutions in the absence of SBDs. The line broadening and the lower peak-to-peak distance in the spectra of SBD solutions, with respect to pure Mn^{2+} solutions, correspond to (a) increase in τ_c corresponding to a slowing down of mobility, (b) decrease in $\langle a \rangle$ corresponding to a decrease in environmental polarity, and (c) increase in **D:D** corresponding to a distortion from cubic symmetry of the solvation shells of Mn(II). On this basis, we suggest that the fraction of Mn^{2+} ions responsible of signal A was localized in the hydration layers of the SBDs in fast exchange with $Mn(H_2O)_6^{2+}$ in the bulk solution. Fast exchange is responsible of averaged parameters, which differ from the parameters of pure Mn(II) solutions.

(2) The **D:D** parameter of spectrum B largely increased with respect to spectrum A. This large **D:D** parameter may be considered as an average of a distribution of ZFS parameters (due to a distribution of sites). Since direct complexation of Mn^{2+} should lead to unobservable EPR spectra (see above), we suggest that spectrum B was due to Mn(II) interacting with the COO^- groups, which partly substitute water molecules in the second−third solvation shells of the ions. The dynamic substitution of water molecules in the second−third solvation shells accounts for the distortion of the cubic symmetry of the Mn−aquo complexes (increase in the **D:D** parameter), which results in the line broadening.[27]

(3) Spectrum A was the minor component. The larger fraction of the ions was involved in the complexation with COO^- groups in the second−third solvation shells.

(4) The increase in generation led to the following effects: (I) A small increase of spectrum B at the expenses of A at pH = 7, whereas the opposite held at pH = 4. This behavior may be connected to the different protonation at the two pH values. The high protonation of NR_3 groups, internally to the SBD structure, at pH = 4 neutralized the negative charge density at the external surface and partially prevented the Mn(II) ions to interact with the SBD-COO^- groups. This behavior mainly holds for the later generation dendrimers, since with the increase in generation, the external layers of the SBD becomes more and more congested (packed)[6] and, consequently, the charge density increases.

Since all the EPR measurements were performed at the same SBD-COO^- concentration (0.37 M), the increase in percentage of spectrum B at pH = 7 for later generations, with respect to the earlier generations, was ascribed to the larger charge density of the later generation, due to the high packing of the surface groups. (II) The $\langle a \rangle$ value of spectrum A decreased from 3.5-SBD to 5.5-SBD and then increased up to G = 7.5. We assumed that the Mn(II) ions responsible for spectrum A were localized (in fast exchange with the external bulk solution) close to less polar SBD sites (like the CCH_2CH_2N chains), and therefore the $\langle a \rangle$ value decreased. (III) At G = 7.5 and low pH, the high packing of the external layer of the dendrimer, and the higher concentration of positively charged NR_3H^+, partly prevented both the entrance of the Mn(II) inside the SBD structure and the formation of Mn(II) complexes responsible for spectrum B. Thus, the relatively high $\langle a \rangle$ for Mn(II) in 7.5-SBD solutions probably arose from the location of the ions in vicinity of the charged SBD-COO^- groups, which led to the increase in the environmental polarity of $Mn(H_2O)_6^{2+}$.

To better visualize the suggested location of Mn(II) in the various experimental conditions, Figure 3 shows the bidimensional projections of *n*.5-SBDs in two rather different situations: (a) G = 3.5 and pH = 7. The open structure of this early generation dendrimer allowed the partial insertion of Mn(II) inside the SBD cavities, in fast exchange with the external solution, of the Mn_{aq} ions generating signal A. At pH = 7 only the first layer of NR_3 groups was protonated; therefore the negative charge of the SBD-COO^- groups was not neutralized and a large portion (80%) of Mn_{aq} ions directly interacted (signal B) with the carboxylate groups. (b) G = 7.5 and pH = 4. The closed surface structure of this later generation dendrimer and the high degree of protonation partially prevented the interaction of Mn_{aq} ions with the SBD-COO^- at the second solvation shell (signal B). However, the Mn(II) aquo ions responsible for signal A experienced a higher environmental polarity due to the higher charge density at the surface of later generation SBDs with respect to the earlier generations.

In Figure 3 the main experimental results that support the above conclusions are also summarized.

Variation of the Line Width of the Fourth Hyperfine Component in the Mn(II) EPR Spectra (Spectrum A) as a Function of pH and Generation. The broadening of the 4th

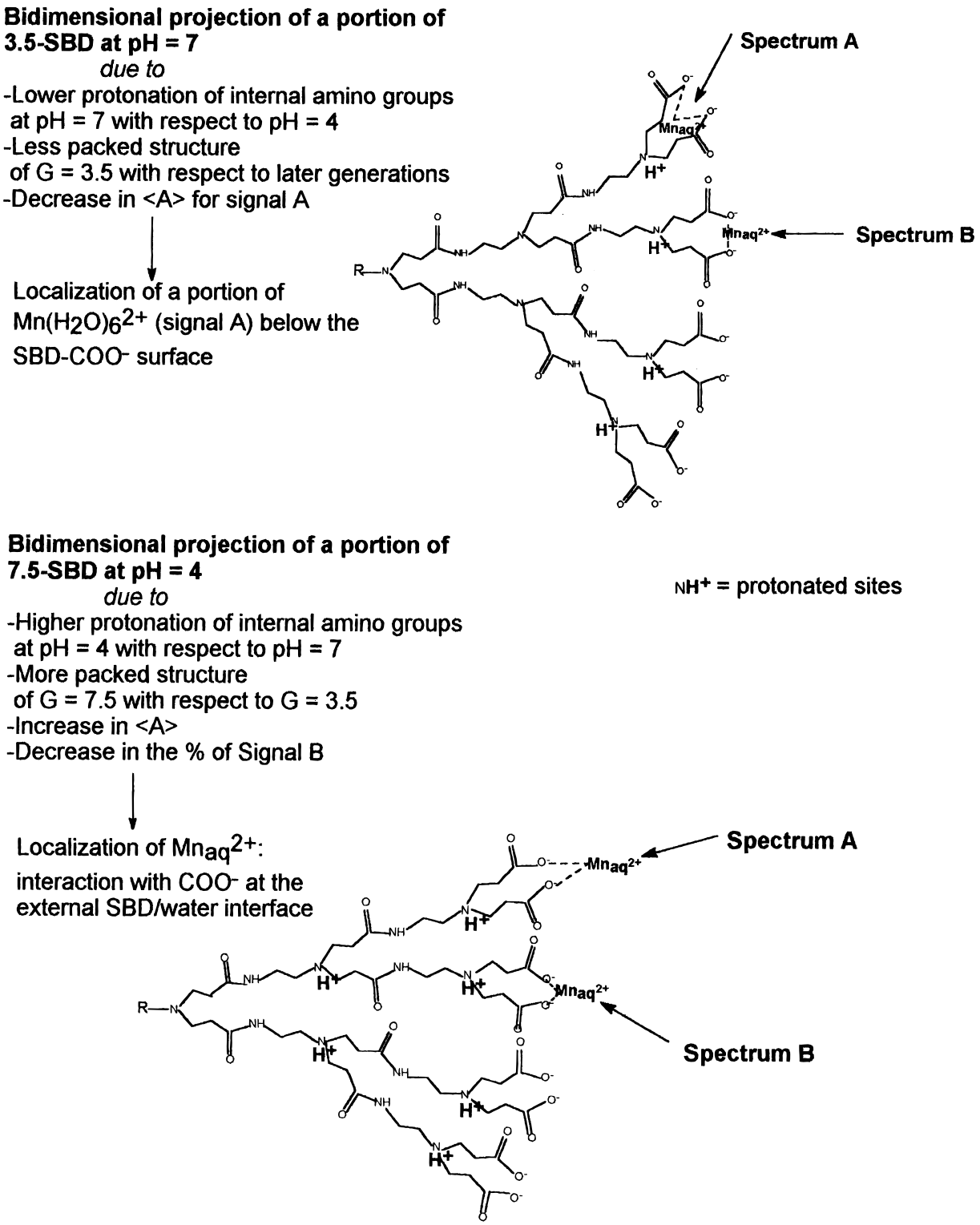

Figure 3. Bidimensional projections of a portion of *n*.5-SBD at $G = 3.5$ and pH = 7, and at $G = 7.5$ and pH = 4. The suggested locations of $Mn(H_2O)_6^{2+}$ are indicated, which correspond to specrum A and spectrum B. The main experimental results that support the hypothesis of Mn(II) location are also reported.

hyperfine component, ΔH_{IV}, of the Mn(II) solution spectra at room temperature has often been used to indicate the complexation of Mn_{aq} ions.[21,37] The choice of the fourth line arises from the narrower width with respect to the other hpf lines, since the five fine adsorptions ($S = {}^5/_2$) fall in a very narrow field range.[28] Therefore, the fourth hyperfine component of the Mn(II) EPR spectra is poorly affected by second-order effects in the line width calculation.[26−28] However, on the basis of eq 2, both variations of **D:D** (in the range $(1-7) \times 10^4$ G^2) and τ_c affect the width of the fourth hpf line. Mainly, ΔH_{IV} is used as a sensitive parameter for structural modification of the Mn(II) environment. The increase in ΔH_{IV} reflects the progressive distortion of the geometry of the Mn_{aq} complex from the cubic symmetry (**D:D** variations).

Figure 4 reports the variation in ΔH_{IV} as a function of pH for a solution of Mn(II) (4×10^{-4} M) containing 7.5-SBD ([SBD-COO$^-$] = 0.37 M). The line width increased with the increase in pH, but a small plateau, corresponding to a variation of slope, was found between pH = 4 and 5, which coincided with the protonation of NR_3 groups below the first NR_3 layer

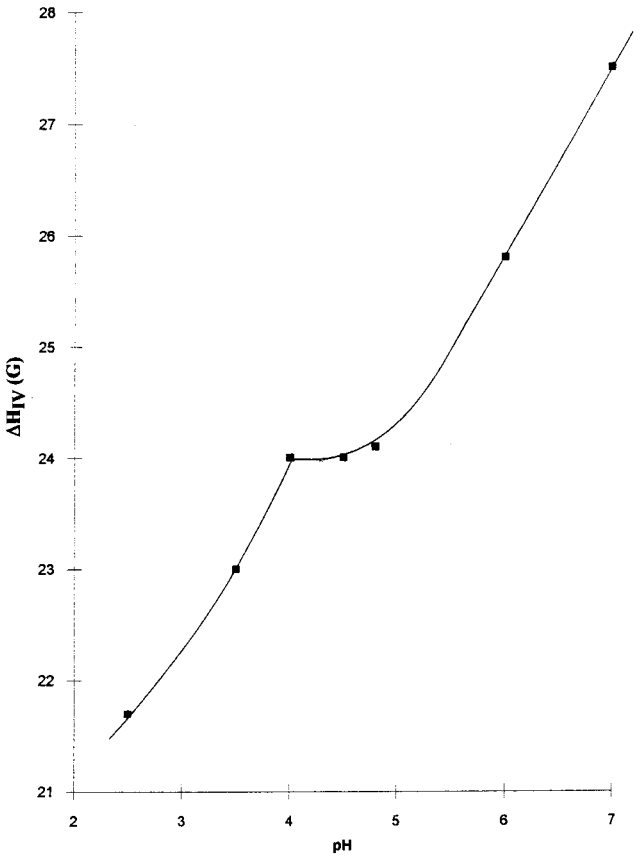

Figure 4. Variation in the line width of the fourth hyperfine component in Mn(II) spectra (ΔH_{IV}) as a function of pH for a Mn(II) solution (4×10^{-4} M) containing 7.5-SBD, at [SBD-COO^-] = 0.37 M.

TABLE 3: ΔH_{IV} Values (Accuracy 5%) for Mn(II) Solutions (2×10^{-4} M) in the Absence and in the Presence of *n*.5-SBDs ([SBD-COO^-] = 0.37 M), at pH = 7 and 4

SBD	pH	ΔH_{IV} (*G*)	SBD	pH	ΔH_{IV} (*G*)
no	7	20.0	no	4	22.5
3.5	7	25.0	3.5	4	23.0
5.5	7	26.0	5.5	4	24.0
7.5	7	27.5	7.5	4	24.0

($G = 7$). This result supports the assumption made on the basis of Figure 3 that the positive charge of the dendrimers at low pH does not allow the Mn(II) to exchange between the internal and the external hydration layers of the SBD. Only at pH > 5 does the progressive deprotonation of the internal NR_3 shells favor the interaction of Mn(II) with the SBD-COO^- groups, which corresponded to the increase in ΔH_{IV}.

Table 3 reports the ΔH_{IV} values for Mn(II) solutions (2×10^{-4} M) in the absence and in the presence of 3.5-, 5.5-, and 7.5-SBDs ([SBD-COO^-] = 0.37 M), at pH = 7 and 4. First, ΔH_{IV} of water solutions of Mn(II) were different for the two pH values. The larger value found at pH = 4 was probably due to the addition of HCl, which also provided a new Mn(II) ligand, Cl^-. When the Cl^- ions are colliding with the Mn−aquo complex, the dynamic substitution of water molecules in the second−third solvation shells of the ions leads to the increase in the **D:D** parameter, which results in the line broadening.[27] The addition of the dendrimers in solution provoked the increase in ΔH_{IV} from 20 to 26−28 G at pH 7, whereas at pH 4 the variation of ΔH_{IV} upon addition of the SBDs was almost negligible (from 22.5 G, in the absence of the dendrimers, to 24 G for 7.5-SBD solutions). We hypothesize that the Cl^- ions in the second solvation shell around the Mn(II) ions were in part replaced by the SBD-COO^- groups with almost no variation of the ZFS parameters. However, the increase in generation from 3.5 to 7.5 led to a variation of ΔH_{IV} of about 2 G, which accounted for the constant *D* parameter of spectrum A at various generations.

Analysis of the EPR Spectra as a Function of Temperature. Figure 5 shows two representative series of EPR spectra of Mn^{2+}−*n*.5-SBD systems as a function of decreasing temperature. In particular, Figure 5a shows the spectra of Mn^{2+} (2×10^{-4} M) in a solution of 3.5-SBD (0.37 M) at pH = 7, in the temperature range between 303 and 218 K; Figure 5b shows the spectra of Mn^{2+} (4×10^{-4} M) in a solution of 7.5-SBD (0.37 M) at pH = 7, in the temperature range between 298 and 218 K. Liquidlike spectra were observed at $T > 255$ K for the 3.5-SBD solution and at $T > 263$ K for the 7.5-SBD solutions. In the liquidlike spectra, a progressive increase in line width was observed with the decrease of *T*, but no maximum of line width was reached, as expected for the condition $\omega_o^2\tau_c^2 = 1$ (see the section on Analysis of the EPR Spectra). The solutions of 3.5-SBD at 255 K, and of 7.5-SBD at 263 K, showed a freezing transition of a fraction of the Mn(II) solution. Consequently, a component of the EPR signal "disappeared". The remaining portion of Mn(II) solution showed a progressive variation toward a solidlike spectrum with further decreases in temperature, and at 218 K the forbidden transitions were clearly recognized in the EPR spectra, which were typical of $Mn(H_2O)_6^{2+}$ in a glassy matrix.[35] We hypothesized that the fraction of Mn(II)−aquo ions, in a glassy environment at low temperature, corresponded to the Mn(II) ions responsible for spectrum B, that is, the "interacting fraction", whereas the portion of solution that underwent crystallization was, at least in part, responsible for signal A, that is, the "free-Mn fraction". Indeed, the integrated intensities of the spectra above and below the crystallization temperature provided the relative percentages of the interacting and free-Mn fractions, which agreed well with the percentages reported for signals B and A, respectively, in Table 2. We expected that the relative intensity of the free-Mn fraction nullified at a certain temperature due to the freezing of this fraction of solution. On the contrary, in some cases, the relative intensity of the free-Mn fraction (evaluated from computation) gradually decreased with the decrease in temperature. This is shown in Figure 6, which reports the variation in the relative intensity of free Mn, normalized at the same maximum value, as a function of temperature for Mn^{2+} (4×10^{-4} M) solutions containing 7.5-SBD (0.37 M) at pH = 7, 4.5, and 2.5. The analysis of the spectral features in Figure 5, and the graph in Figure 6, provided the following findings:

(i) The freezing temperature of the free-Mn fraction is lower for the earlier generations with respect to the later generations at pH = 7. Similar behavior has been described for the positively charged nitroxide radical, CAT1, in solutions of *n*.5-SBDs.[12] The open external conformation of the earlier generation dendrimers[6] favored the entering of the free Mn(II) into the SBD structure. The water solution in the internal pools of the SBDs was frozen at lower temperature with respect to the external water. It is noteworthy that at pH = 4 the transition temperature was almost the same (about 268 K) for earlier and later generations, which further indicated that the protonation of the internal NR_3 groups prevented the Mn(II) from entering inside the SBD structure.

(ii) The so-called interacting fraction of Mn(II) corresponded to manganous ions localized in the hydration layers at the surface of the SBDs, the SBD-COO^- groups substituting water molecules in the second solvation shell of the ions. The rheological properties of this hydration water were modified and a glass

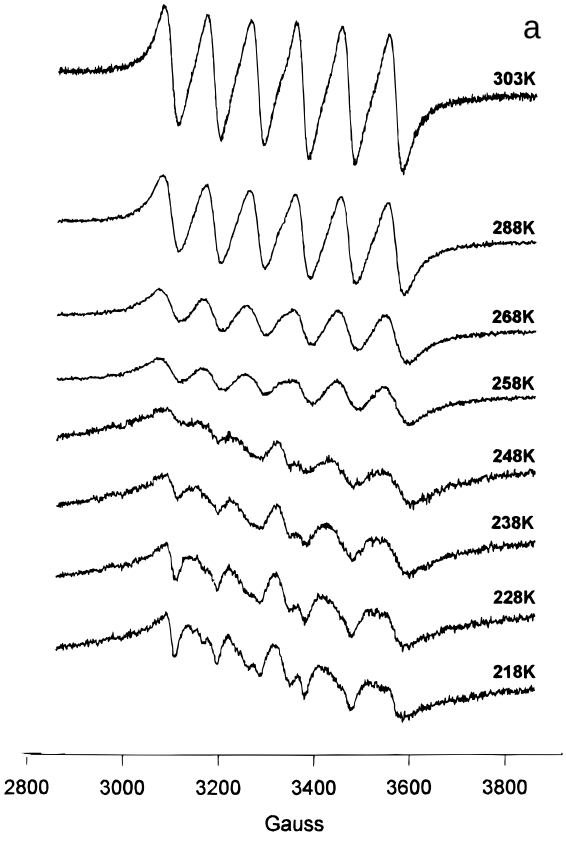

Figure 5. (a) EPR spectra of Mn^{2+} (2×10^{-4} M) in a solution of 3.5-SBD (0.37 M) at pH = 7, in the temperature range between 218 and 303 K; (b) EPR spectra of Mn^{2+} (4×10^{-4} M) in a solution of 7.5-SBD (0.37 M) at pH = 7, in the temperature range between 218 and 298 K.

transition was found, similar to that shown for water confined in microheterogeneous systems, such as water solutions adsorbed onto porous supports.[22,38−44]

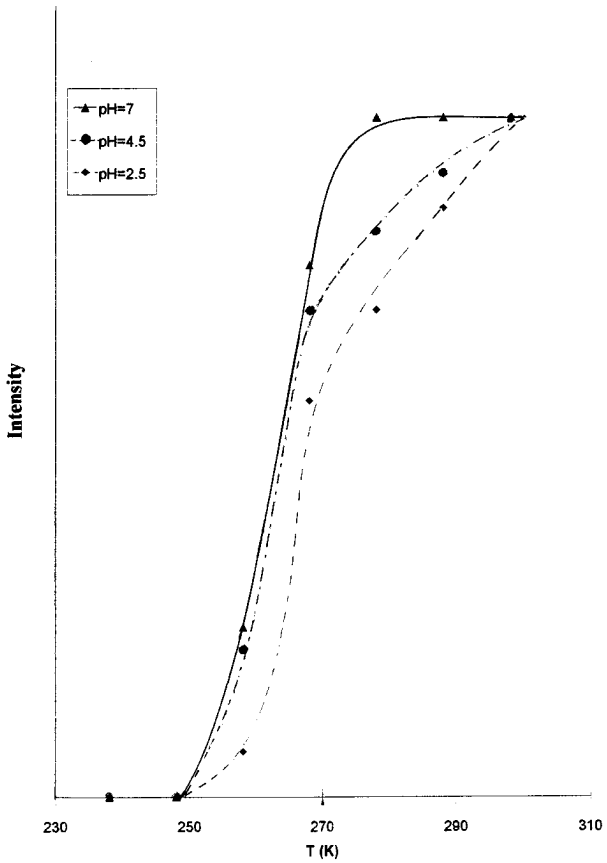

Figure 6. Variation in the relative intensity of the EPR signal of free Mn as a function of temperature, for Mn^{2+} (4×10^{-4} M) solutions containing 7.5-SBD (0.37 M) at pH = 7, 4.5, and 2.5 (normalized at the same maximum intensity value).

(iii) The decrease in the intensity of the free-Mn components with the decrease in temperature was more gradual at pH = 4.5 and 2.5 if compared with the decrease at pH = 7 (Figure 6). The gradual freezing was clearly due to a distribution of sites occupied by the Mn(II) at the SBD/water interface.

(iv) At high pH, the small fraction of free Mn underwent freezing at an almost constant temperature. A very narrow distribution of sites may explain this behavior.

EPR Spectra of Mn(II)−*n*.5-SBD Systems at Different Concentrations of the Components. The increase in the concentration of Mn(II), at constant SBD-COO^- concentration, led to the same effect as a decrease in [SBD-COO^-] at constant [Mn^{2+}]. Figure 7 shows the EPR spectra (298 K) of 7.5-SBD solutions (0.37 M in SBD-COO^-) at pH = 7 and 4, containing Mn(II) at concentrations of 2×10^{-4} (full lines) and 6×10^{-4} M (dashed lines). The behavior may be elucidated in terms of the following reaction:

$$n\mathrm{Mn(H_2O)_6}^{2+} + m\mathrm{H_2O} + n^{-}\mathrm{OOC\text{-}SBD} \rightarrow m\mathrm{Mn(H_2O)_6}^{2+}\cdots\mathrm{H_2O}\cdots{}^{-}\mathrm{OOC\text{-}SBD} + (n-m)\mathrm{Mn(H_2O)_6}^{2+}\cdots{}^{-}\mathrm{OOC\text{-}SBD} \quad (4)$$

The above equation is interpreted in terms of a distribution of Mn(II) in solution between two environments: the species $Mn(H_2O)_6^{2+}\cdots H_2O\cdots{}^{-}$OOC-SBD are responsible for spectrum A, whereas spectrum B arises from the species $Mn(H_2O)_6^{2+}\cdots{}^{-}$OOC-SBD (see Figure 2). The analysis of Figure 7 indicated that the addition of increasing amounts of Mn^{2+} in the dendrimer solution corresponded to an increase in $Mn(H_2O)_6^{2+}\cdots H_2O\cdots{}^{-}$OOC-SBD, whereas the complex $Mn(H_2O)_6^{2+}\cdots{}^{-}$OOC-SBD relatively diminished in solution.

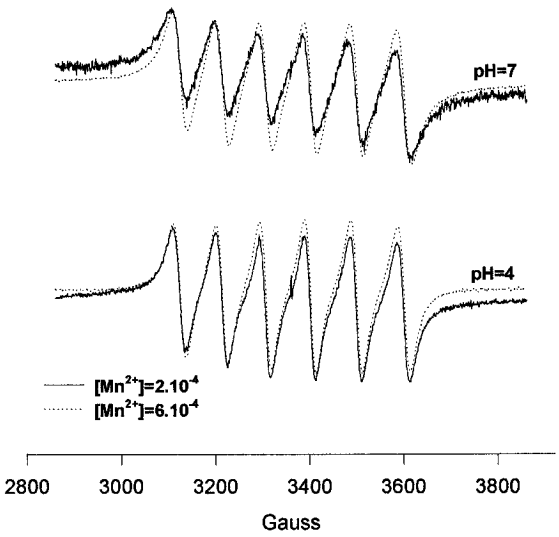

Figure 7. EPR spectra (298 K) of 7.5-SBD solutions (0.37 M in SBD-COO^-) at pH = 7 and 4, containing Mn(II) at concentrations of 2×10^{-4} (full lines) and 6×10^{-4} M (dashed lines).

The same effect was obtained by decreasing the carboxylate concentration. The spectra in Figure 7 for $[Mn^{2+}] = 6 \times 10^{-4}$ M were computed by using the same D, τ_c, and $\langle a \rangle$ parameters, as for $[Mn^{2+}] = 2 \times 10^{-4}$ M at equivalent pH and generation (Table 2). However, the percentages of the two components, spectrum A and spectrum B, contributing to the overall EPR signal, were different for the two different Mn(II) concentrations. If we assume that all the Mn(II) in solution is present either as $Mn(H_2O)_6^{2+}\cdots H_2O\cdots{}^-OOC$-SBD (spectrum A) or as $Mn(H_2O)_6^{2+}\cdots{}^-OOC$-SBD (spectrum B), the percentages of the two signals (A and B) provided the concentrations of the two components in the SBD solution:

$[Mn^{2+}]$ $\times 10^4$ (M)	pH	species	concn (M)
2	7	$Mn(H_2O)_6^{2+}\cdots H_2O\cdots{}^-OOC$-SBD	3.0×10^{-5}
		$Mn(H_2O)_6^{2+}\cdots{}^-OOC$-SBD	1.7×10^{-4}
6	7	$Mn(H_2O)_6^{2+}\cdots H_2O\cdots{}^-OOC$-SBD	3.0×10^{-4}
		$Mn(H_2O)_6^{2+}\cdots{}^-OOC$-SBD	3.0×10^{-4}
2	4	$Mn(H_2O)_6^{2+}\cdots H_2O\cdots{}^-OOC$-SBD	8.0×10^{-5}
		$Mn(H_2O)_6^{2+}\cdots H_2O\cdots{}^-OOC$-SBD	8.0×10^{-5}
6	4	$Mn(H_2O)_6^{2+}\cdots H_2O\cdots{}^-OOC$-SBD	4.8×10^{-4}
		$Mn(H_2O)_6^{2+}\cdots{}^-OOC$-SBD	1.2×10^{-4}

Therefore the $Mn(H_2O)_6^{2+}$ directly complexed by the SBD-COO^- increased in concentration very slightly with the increase in the total $[Mn^{2+}]$. This finding may be described in terms of a "saturation" of the complexing sites at the surface of the dendrimers by the interacting $Mn(H_2O)_6^{2+}$. Since the concentration in SBD-COO^- was 0.37 M, the saturation should correspond to a maximum of 0.05−0.1% of the carboxylate groups involved in the complexation.

Conclusions

Mn(II) has been shown to be a good EPR probe to investigate the interacting abilities of the various ligand sites on the surface of SBDs at different protonation conditions, and as a function of generation (G), for both half and full generation SBDs (n.5-SBDs and n-SBDs, respectively). The computer-aided analysis of the EPR spectra of Mn(II) provided information on the location of Mn(II) in the hydration layers of the internal and external SBD surface and on the physical status of water inside the dendrimer structure and at the surface/solution interface. Mn(II) did not show any interaction with the full-generation dendrimers and only interacted, probably at the second solvation shell, with the surface carboxylate groups (SBD-COO^-) of n.5-SBDs. Spectral analysis was simplified by considering that two main components constituted the EPR spectra, arising from Mn^{2+} in two different environments in slow exchange with each other in the EPR time scale: (1) A minor component, termed spectrum A, was due to Mn(II) that is located in the solvation shells of the SBD surface in fast exchange with the bulk solution. At high pH, mainly for the more open surfaced earlier generation dendrimers ($G < 4.5$), the Mn−aquo complexes converged close to internal SBD sites of low polarity. On the contrary, the dense packing of the external layer of the later generation dendrimers ($G > 4.5$), and the high concentration of the NR_3H^+ groups, at the interior layers of the SBD structure at low pH, in part prevented the entrance of $Mn(H_2O)_6^{2+}$ inside the SBD structure. This Mn(II) fraction underwent the freezing transition at about 255 K. However, samples at low pH showed the freezing transition in a large range of temperatures, due to a distribution of sites occupied by Mn(II) at the SBD/water interface. (2) The major component, termed spectrum B, arose from complexation of Mn(II) with SBD-COO^- groups. The distortion from cubic symmetry of the Mn(II) environment indicated that water molecules belonging to the second solvation shell of the ions were substituted by COO^- groups. This "interacting" fraction of Mn(II) was larger for later generation, due to the larger charge density compared to the earlier generations. The portion of solution that contained the Mn(II) complexes underwent a glass transition with the decrease in temperature. This result indicated that the rheological properties of water in the vicinity of the SBD surface were modified, as is usually found for water trapped in microheterogeneous structures.

The fraction of Mn(II) generating spectrum B reached a maximum with the increase in Mn(II) concentration. It was assumed that all the Mn(II) in solution was present either as $Mn(H_2O)_6^{2+}\cdots H_2O\cdots{}^-OOC$-SBD (spectrum A) or as $Mn(H_2O)_6^{2+}\cdots{}^-OOC$-SBD (spectrum B). On the basis of the analysis of the EPR spectra, the maximum of carboxylate groups involved in the direct complexation of $Mn(H_2O)_6^{2+}$ (spectrum B) was 0.05−0.1%.

Acknowledgment. N.J.T. thanks the AFOSR and NSF for their generous support. D.A.T. thanks the New Energy and Development Organization (NEDO) of the Ministry of International Trade and Industry of Japan (MITI) for the generous support and certain critical synthetic efforts. M.F.O. and F.M. thank the Italian Ministero Università e Ricerca Scientifica e Tecnologica (MURST) and the Italian Consiglio Nazionale delle Ricerche (CNR) for the financial support.

References and Notes

(1) *Advances in Dendritic Macromolecules*; Newkome, G. R., Ed; JAI Press: Greenwich CT, 1993.

(2) (a) Krohn, K, Starburst Dendrimers and Arborols. In *Organic Synthesis Highlights*; Mulzer, J., et al., Eds.; VCH: Weinheim, 1991; p 378. (b) Amato, L. Trekking in the Molecular Forest. *Sci. News* **1990**, *138*, 298.

(3) (a) Newkome, G. R.; Moorefield, C. N.; Baker, G. R.; Johnson, A. L.; Behera, R. K. *Angew. Chem., Int. Ed. Engl.* **1991**, *30*, 1176. (b) Newkome, G. R.; Moorefield, C. N.; Baker, G. R.; Saunders, M. J.; Grossman, S. H. *Angew. Chem., Int. Ed. Engl.* **1991**, *30*, 1178. (c) Newkome, G. R.; Young, J. K.; Baker, G. R.; Potter, R. L.; Audoly, L; Cooper, D.; Weis, C. D. *Macromolecules* **1993**, *26*, 2394.

(4) (a) Kim, Y. H.; Webster, O. W. *J. Am. Chem. Soc.* **1990**, *112*, 4592. (b) Hawker, C. J.; Wooley, K. L.; Fréchet, J. M. J. *J. Chem. Soc., Perkin Trans. 1* **1993**, 1287. (c) Frechet, J. M. J. *Science* **1994**, *263*, 1710. (d) Jansen, J. F. G. A.; deBrabander-Van de Berg, E. M. M.; Meijer, E. W. *Science* **1994**, *266*, 1226.

(5) (a) Tomalia, D. A.; Baker, H.; Dewald, J; Hall, M.; Kallos, G.; Martin, S.; Roeck, J.; Smith, P. *Polym. J. (Tokyo)* **1985**, *17*, 117. (b) *Macromolecules* **1986**, *19*, 2466. (c) Tomalia, D. A.; Berry, V.; Hall, M.; Hedstrand, D. M. *Macromolecules* **1987**, *20*, 1164. (d) Tomalia, D. A.;

Hall, M.; Hedstrand, D. M. *J. Am. Chem. Soc.* **1987**, *109*, 1601. (e) Padias, A. B.; Hall, H. K.; Tomalia, D. A.; McConnell, J. R. *J. Org. Chem.* **1987**, *52*, 5305. (f) Wilson, L. R.; Tomalia, D. A. *Polym. Prepr. (Am. Chem. Soc., Div. Polym. Chem.)* **1989**, *30*, 115. (g) Padias, A. B.; Hall, H. K.; Tomalia, D. A. *Polym. Prepr. (Am. Chem. Soc., Div. Polym. Chem.)* **1989**, *30*, 119. (h) Tomalia, D. A.; Naylor, A. M.; Goddard, W. A., III *Angew Chem., Int. Ed. Engl.* **1990**, *29*, 138. (i) Tomalia, D. A.; Dewald, J. R. U.S. Patent 4 507 466, 1985; U.S. Patent 4 558 120, 1985; U.S. Patent 4, 568, 737, 1986; U.S. Patent 4, 587, 329, 1986; U.S. Patent 4, 631, 337, 1986; U.S. Patent 4, 694, 064, 1986; U.S. Patent 4, 857, 599, 1989.

(6) Naylor, A. M.; Goddard, W. A., III; Kiefer, G. E.; Tomalia, D. A. *J. Am. Chem. Soc.* **1989**, *111*, 2341.

(7) Smith, P. B.; Martin, S. J.; Hall, M. J.; Tomalia, D. A. In *Applied Polymer Analysis and Characterization*; Mitchell, J., Jr., Ed.; Hanser: Munchen/New York, 1987; p 357.

(8) Meltzer, A. D.; Tirell, D. A.; Jones, A. A.; Inglefield, P. T.; Downing, D. M.; Tomalia, D. A. *Polym. Prepr. (Am. Chem. Soc., Div. Polym. Chem.)* **1989**, *30*, 121.

(9) Moreno-Bondi, M.; Orellana, G.; Turro, N. J.; Tomalia, D. A. *Macromolecules* **1990**, *23*, 910.

(10) Gopidas, K. R.; Leheny, A. R.; Caminati, G.; Turro, N. J.; Tomalia, D. A. *J. Am. Chem. Soc.* **1991**, *113*, 7335.

(11) Caminati, G.; Turro, N. J.; Tomalia, D. A. *J. Am. Chem. Soc.* **1990**, *112*, 8515.

(12) Ottaviani, M. F.; Cossu, E.; Turro, N. J.; Tomalia, D. A. *J. Am. Chem. Soc.* **1995**, *117*, 4387.

(13) Ottaviani, M. F.; Turro, N. J.; Jockusch, S.; Tomalia, D. A. *J. Phys. Chem.*, in press.

(14) Ottaviani, M. F.; Bossmann, S.; Turro, N. J.; Tomalia, D. A. *J. Am. Chem. Soc.* **1994**, *116*, 661.

(15) Rubinstein, M; Baram, A.; Luz, Z. *Mol. Phys.* **1971**, *20*, 67.

(16) Garrett, B. B.; Morgan, L. O. *J. Chem. Phys.* **1966**, *44*, 890.

(17) Levanon, H.; Stein, G.; Luz, Z. *J. Chem. Phys.* **1970**, *53*, 3056.

(18) Martini, G.; Romanelli, M.; Burlamacchi, L. In *Molecular Motions in Liquids*; Lascombe, J., Ed.; Reidel: Dordrecht, The Netherlands, 1974; p 371.

(19) Hayes, R. G.; Myers, R. J. *J. Chem. Phys.* **1964**, *40*, 877.

(20) Nuti, L.; Ottaviani, M. F. *J. Phys. Chem.* **1985**, *89*, 4773.

(21) (a) Burlamacchi, L.; Martini, G.; Ottaviani, M. F. *J. Chem Soc., Faraday Trans. 2* **1976**, *72*, 324. (b) Burlamacchi, L. *J. Chem. Soc., Faraday Trans. 2* **1975**, *71*, 54.

(22) Ottaviani, M. F.; Mello-Ceresa, E.; Visca, M. *J. Colloid Interface Sci.* **1985**, *108*, 114.

(23) Burlamacchi, L.; Ottaviani, M. F.; Mello-Ceresa, E.; Visca, M *Colloid Surf.* **1983**, *7*, 165.

(24) Duczmal, T.; Buckmaster, H. A. *Appl. Clay Sci.* **1987**, *2*, 273.

(25) Kudynska, J.; Duczmal, T.; Buckmaster, H. A. *Appl. Clay Sci.* **1989**, *4*, 225.

(26) McGarvey, B. R. *J. Phys. Chem.* **1957**, *61*, 1232.

(27) Burlamacchi, L.; Martini, G.; Ottaviani, M. F.; Romanelli, M. *Adv. Mol. Relax. Interact. Processes* **1978**, *12*, 145.

(28) (a) Lewis, W. B.; Morgan, L. O. In *Transition Metal Chemistry*; Carlin, R. L., Ed.; Marcel Dekker: New York, 1968; Vol. 4, p 33. (b) Bloembergen, N.; Morgan, L. O. *J. Chem. Phys.* **1961**, *34*, 842.

(29) Atherton, N. M. In *Electron Spin Resonance*; Horwood, E., Ed.; J. Wiley: New York, 1973.

(30) Luckhurst, G. R.; Pedulli, G. F. *Chem. Phys. Lett.* **1970**, *7*, 49.

(31) Luckhurst, G. R.; Pedulli, G. F. *Mol. Phys.* **1971**, *22*, 931.

(32) Tsay, F. D.; Manatt, S. L.; Chan, S. I. *Chem. Phys. Lett.* **1972**, *17*, 223.

(33) Romanelli, M.; Burlamacchi, L. *Mol. Phys.* **1976**, *31*, 115.

(34) Romanelli, M.; Burlamacchi, L. *J. Chem. Phys.* **1973**, *58*, 3609.

(35) Kindly provided by Prof. M. Mascini, University of Florence.

(36) *Introduction to Organic Chemistry*; Streitweiser, A., Heathcock, C. H., Kosover, E. M., Eds.; MacMillan: New York, 1992.

(37) Ristori, S.; Ottomani, E.; Romanelli, M.; Martini, G. *J. Phys. Chem.* **1995**, *99*, 17886.

(38) Bassetti, V.; Burlamacchi, L.; Martini, G. *J. Am. Chem. Soc.* **1979**, *101*, 5471.

(39) Martini, G.; Ottaviani, M. F.; Romanelli, M. *J. Colloid Interface Sci.* **1983**, *94*, 105.

(40) Pearson, R. T.; Derbyshire, J. C. *J. Colloid Interface Sci.* **1974**, *46*, 232.

(41) Etzler,F. M.; Fagundus,D. M. *J. Colloid Interface Sci.* **1987**, *115*, 513.

(42) Ramsey, J. D. F.; Poisignon, C *Langmuir* **1987**, *3*, 320.

(43) Belfort, G.; Scherfig, J.; Seevers, D. O. *J. Colloid Interface Sci.* **1974**, *47*, 106.

(44) Villa, M.; Borghi, L.; De Ambrosis, A.; Aldrovandi, S. *Nuovo Cimento* **1983**, *2D*, 1019.

JP953261H